A Progress Report

to

Dr. Donald J. Silversmith
Dr. Kitt Reinhardt
Air Force Office of Scientific Research

Development of Advanced III-Nitride Materials

AFOSR Program # FA9550-08-1-0461

James S. Speck

Materials Department
University of California
Santa Barbara, CA 93106

Report Documentation Page

Form Approved
OMB No. 0704-0188

Public reporting burden for the collection of information is estimated to average 1 hour per response, including the time for reviewing instructions, searching existing data sources, gathering and maintaining the data needed, and completing and reviewing the collection of information. Send comments regarding this burden estimate or any other aspect of this collection of information, including suggestions for reducing this burden, to Washington Headquarters Services, Directorate for Information Operations and Reports, 1215 Jefferson Davis Highway, Suite 1204, Arlington VA 22202-4302. Respondents should be aware that notwithstanding any other provision of law, no person shall be subject to a penalty for failing to comply with a collection of information if it does not display a currently valid OMB control number.

1. REPORT DATE **24 SEP 2008**	2. REPORT TYPE	3. DATES COVERED

4. TITLE AND SUBTITLE **Development Of Advanced III-Nitride Materials**	5a. CONTRACT NUMBER 5b. GRANT NUMBER 5c. PROGRAM ELEMENT NUMBER
6. AUTHOR(S)	5d. PROJECT NUMBER 5e. TASK NUMBER 5f. WORK UNIT NUMBER
7. PERFORMING ORGANIZATION NAME(S) AND ADDRESS(ES) **The Regents Of The University of California-Santa Barbara,Department of Engineering - Materials,Engrng Ii, Bldg 503, Rm, 1347c,Santa Barbara,CA,93106**	8. PERFORMING ORGANIZATION REPORT NUMBER
9. SPONSORING/MONITORING AGENCY NAME(S) AND ADDRESS(ES)	10. SPONSOR/MONITOR'S ACRONYM(S) 11. SPONSOR/MONITOR'S REPORT NUMBER(S)

12. DISTRIBUTION/AVAILABILITY STATEMENT
Approved for public release; distribution unlimited.

13. SUPPLEMENTARY NOTES
The original document contains color images.

14. ABSTRACT

15. SUBJECT TERMS

16. SECURITY CLASSIFICATION OF:			17. LIMITATION OF ABSTRACT	18. NUMBER OF PAGES	19a. NAME OF RESPONSIBLE PERSON
a. REPORT **unclassified**	b. ABSTRACT **unclassified**	c. THIS PAGE **unclassified**		**15**	

Standard Form 298 (Rev. 8-98)
Prescribed by ANSI Std Z39-18

Objectives

This new AFOSR program is focused on basic issues in the growth of advanced GaN and InN-based materials by molecular beam epitaxy (MBE). Work is focused on three areas: (i) extend on our pioneering work on high temperature nitrogen-rich growth of GaN, where we have demonstrated a new growth space for realizing high quality GaN materials and devices including world record room bulk electron mobility in GaN by MOCVD or MBE; (ii) continue our work on InN and its alloys with a particular emphasis on realizing p-type doping, p-n junctions, and InGaN/InN quantum well structures for terahertz emitters; and (iii) develop AlInN materials lattice-matched to GaN for advanced optoelectronic emitters and electron devices.

Progress

High Temperature N-rich GaN Growth

We have continued to explore high temperature N-rich plasma-assisted MBE (PAMBE) growth of GaN. In conventional GaN PAMBE growth, the highest quality materials and highest performance devices have been realized by metal-rich growth. Under metal-rich growth, the GaN surface is covered by a Ga wetting layer (2.5 ML's thick) and additionally Ga droplets that degrade the film morphology. Under previous AFOSR support we demonstrated a new high temperature N-rich growth regime that unexpectedly yielded GaN with world record room temperature mobilities and high demonstrated high performance high electron mobility transistors.

In the current program, we are continuing to explore physical properties of PAMBE of GaN grown at high temperatures. We have collaborated with Prof. Ed Yu's group at UC San Diego on conductive atomic force microscopy (CAFM). Conductive atomic force microscopy and cross-sectional transmission electron microscopy were used to determine the effects of Ga-to-N adatom flux at elevated growth temperatures on the formation and conductive behavior of threading screw dislocations in gallium nitride grown by molecular-beam epitaxy. The data reveal a narrow band of fluxes near Ga flux/N flux > 1 where threading become very weka leakage pathways. We show that a lack of reverse bias leakage paths is directly correlated with the reduction of leakage associated with of screw-component dislocations. The reduction of reverse bias leakage while simultaneously maintaining high carrier mobility could lead to higher efficiency, power, and speed devices based on the III-nitride materials system. A paper is in final preparation for submission and will be provided to AFOSR upon completion.

We have additionally continued to pursue high temperature N-rich growth using a new plasma source from SVTA (which has promised higher growth rates). We have realized growth rates now up to 1.2 μm/hr with good morphology.

InN Materials

We have continued to work on InN and related materials. During the last year, we have completed many of our basic materials studies and extended our work into nonpolar orientations of InN, as described below.

The role of threading dislocations and unintentional impurities in the bulk conductivity of InN films

The origin of bulk electrons in In-face InN has been studied by considering the effects of both unintentionally incorporated impurities and threading dislocation densities on electron transport properties. The concentration of unintentionally incorporated oxygen and hydrogen scaled with the bulk electron concentration while threading dislocations had no discernable effect on the electron concentration. We conclude that unintentional impurities were the significant source of electrons and threading dislocations acted only as scattering centers limiting the electron mobility in as-grown InN films. Further, we present In-face InN growth techniques controlling the incorporation of oxygen and hydrogen and reducing threading dislocation densities. This work is now published in *Applied Physics Letters* and is given as **Appendix I**.

In adlayer mediated molecular beam epitaxial growth and properties of a-plane InN on freestanding GaN

The role of the In adlayer on the morphological and structural properties of nonpolar *a*-plane InN films was elucidated during the plasma-assisted molecular beam epitaxy on freestanding GaN. Reflection high energy electron diffraction during In adsorption experiments on *a*-plane InN surfaces revealed a stable In adlayer coverage of ~2 ML. This In adlayer-mediated growth was responsible for achieving atomically smooth surfaces (rms roughness <1 nm), phase-pure material with lower x-ray rocking curve widths $\Delta\omega < 0.5°$, lower crystal mosaic tilt/twist, and decreased stacking fault densities, compared to N-rich conditions. The photoluminescence peak emission and band gap energy of the *a*-plane InN films were ~0.63 and ~0.7 eV, respectively. This work is now published in *Applied Physics Letters* and is given as **Appendix II**.

Evaluation of threading dislocation densities in In- and N-face InN

The threading dislocation (TD) structure and density has been studied in In- and N-face InN films grown on GaN by plasma-assisted molecular beam epitaxy. The TD densities were determined by non-destructive x-ray diffraction rocking curve measurements in on-axis symmetric and off-axis skew symmetric geometries and calibrated by by transmission electron microscopy measurements. TD densities were dominated by edge-type TDs with screw-component TDs accounting for less than 10% of the total TD density. InN films grown with excess In and in a high temperature growth regime had the lowest TD densities. The lowest measured TD density for an In-face InN film was $\sim 1.5 \times 10^{10}$ cm^{-2} for 1 μm thick films. This work is in preparation for final submission for publication and will be provided to AFOSR on submission.

The collective body of UCSB work on InN growth and properties will appear in a review chapter in an upcoming edited volume on InN – the final accepted chapter will be sent directly to AFOSR due to its length.

AlInN Materials

We have initiated a major research activity on InAlN materials – both by MOCVD and by MBE (the latter primarily under AFOSR support). InAlN, with an indium content of ~18% is nominally lattice matched to GaN and thus provides a very attractive barrier material for GaN-based HEMTs and also as a refractive index contast material for optoelectronic devices.

Growth of high quality AlN $(000\bar{1})$ on Si(111) by plasma-assisted molecular beam epitaxy
In MBE, the basis of developing high quality InAlN has been built on our work on AlN growth, including recent work on N-face AlN growth on Si(111). High quality N-polar AlN epilayers were grown and characterized on Si(111) substrates by plasma- assisted molecular beam epitaxy as a first step toward growth of N-polar nitrides on Si(111). Polarity inversion to N-face by an optimized predeposition of Al adatoms on the reconstructed 7x7 Si(111) surface was investigated. Al adatoms can saturate the dangling bonds of Si atoms, resulting in growth of AlN in $[000\bar{1}]$ direction on subsequent exposure to N_2 plasma. N-polarity was confirmed by observing strong 3x3 and 6x6 reflection high-energy electron diffraction reconstructions, convergent beam electron diffraction imaging and KOH etching studies. The structural properties were investigated by x-ray diffraction measurements, cross section and plan-view TEM studies. This work is given in a recently published *Applied Physics Letter* in **Appendix III**.

MOCVD growth of metal-face and N-face InAlN
In the MOCVD area, we have already realized high quality AlInN on both group III face (analogous to Ga-face) and N-rich. $In_xAl_{1-x}N$ layers, with $0.09 \leq x \leq 0.23$, were grown on GaN on both the In-polar and N-polar orientations by metal organic chemical vapor deposition (MOCVD). The impact of growth conditions, including temperature and the group-III flow rates, on the surface morphology and indium mole fraction was investigated. In-polar layers had a smooth surface morphology characterized by islands which decreased in size with increasing supersaturation during growth. Smooth N-polar InAlN was achieved through the use of vicinal substrates with misorientation angles of 3° to 5°, and a trend of an increase in step-bunching with decreasing supersaturation was observed for N-polar InAlN layers. The indium incorporation increased with decreasing growth temperature and increasing growth rate for both In-polar and N-polar layers. Indium incorporation efficiency was similar for both orientations on samples which were co-loaded in our reactor. This work is in preparation for final submission for publication and will be provided to AFOSR on submission.

We have additionally initiated major growth efforts on InAlN in both metal-face and N-rich orientations byPAMBE. For N-face materials, the full PAMBE growth parameter

Personnel Supported

Dr. Gregor Koblmueller
Dr. Soojeong Choi
Dr. Oliver Bierwagen

Appendices

Appendix I
"The role of threading dislocations and unintentional impurities in the bulk conductivity of InN films," C.S. Gallinat, G. Koblmueller, J.S. Speck, Appl. Phys. Lett. **95**, 022103 (2009).

Appendix II
"In adlayer mediated molecular beam epitaxial growth and properties of a-plane InN on freestanding GaN," G. Koblmüller, G.D. Metcalfe, M. Wraback, F. Wu, C.S. Gallinat, and J. S. Speck, Appl. Phys. Lett. **94**, 091905 (2009).

Appendix III
"Growth of high quality AlN $(000\bar{1})$ on Si(111) by plasma-assisted molecular beam epitaxy," Sansaptak Dasgupta, F. Wu, J.S. Speck, and U. K. Mishra, **94**, 151906 (2009).

The role of threading dislocations and unintentionally incorporated impurities on the bulk electron conductivity of In-face InN

Chad S. Gallinat,[a] Gregor Koblmüller, and James S. Speck
Materials Department, University of California, Santa Barbara, California 93106-5050, USA

(Received 5 May 2009; accepted 17 June 2009; published online 13 July 2009)

The origin of bulk electrons in In-face InN has been studied by considering the effects of both unintentionally incorporated impurities and threading dislocation densities on electron transport properties. The concentration of unintentionally incorporated oxygen and hydrogen scaled with the bulk electron concentration while threading dislocations had no discernable effect on the electron concentration. We conclude that unintentional impurities were the significant source of electrons and threading dislocations acted only as scattering centers limiting the electron mobility in as-grown InN films. Further, we present In-face InN growth techniques controlling the incorporation of oxygen and hydrogen and reducing threading dislocation densities. © *2009 American Institute of Physics*.
[DOI: 10.1063/1.3173202]

The origin of the high n-type conductivity in unintentionally doped (UID) InN films remains an unresolved issue in nitride research. Some groups contend that threading dislocations (TDs) with dangling bonds contribute electrons (e^-) to InN films and may be the origin of the high e^- concentration in all UID InN films.[1–3] This is highly disputed because TDs in InN have been predicted to be negatively charged,[4] similar to the direct observation of negatively charged TDs in bulk GaN.[5] Piper *et al.*[1] more recently calculated that the formation of positively charged nitrogen vacancies at the cores of TDs in InN are energetically favorable in the absence of impurities, suggesting that TDs are the dominant donor in InN. Lebedev *et al.*[2] used variable temperature Hall measurements to observe a relatively constant sheet density down to ~100 K, which they suggested was evidence of direct carrier generation from TDs. A contrasting report by Thakur *et al.*[6] established the need for negatively charged TDs in InN for charge balance and no correlation was observed between TD density and e^- concentration. Although there is no general agreement on the effect TDs have on the carrier concentration in InN films, there seems to be a consensus that TDs are the dominant scattering center limiting e^- mobility in bulk InN. Look *et al.*[4] first reported on the scattering of e^- by TDs in InN, which was subsequently confirmed by several other groups.[2,6,7]

The roles that native defects play in bulk conductivity have also been debated. Nitrogen vacancies, N antisites, and N interstitials along with the incorporation of excess In or In vacancies have all been suggested as donors in InN.[8–11] Based on electronic structure calculations, however, Stampfl *et al.*[12] showed that ionized impurities such as oxygen and silicon have significantly lower formation energies than native defects and should be shallow donors in InN.

Correlations between e^- concentrations and the unintentionally incorporated impurities oxygen and hydrogen had previously been observed.[4,13] These experimental observations have been verified and explained by a number of electronic structure calculations. Limpijumnong and Van de Walle[14] made the surprising prediction that positively charged hydrogen is the only stable form in InN; thus, hydrogen acts exclusively as a donor in InN. The behavior of hydrogen in InN is different than its behavior in GaN or AlN where it behaves as an amphoteric dopant that compensates the prevailing conductivity.[14–16] Most recently, Janotti and Van de Walle[17] explored the role of interstitial hydrogen (H_i) as opposed to substitutional hydrogen on a N site (H_N). They found that the H_N impurity not only had a higher barrier to migration than H_i, but they also observed that H_N actually contributed two e^- to the conduction band.[17] Unintentionally incorporated impurities such as oxygen and, to an even greater extent, hydrogen are potentially significant hurdles in achieving InN with low e^- concentrations or p-type doping. In this work, we correlate the effects of different plasma-assisted molecular beam epitaxy (PAMBE) growth conditions on the transport properties of InN, the structural quality of InN, and the incorporation of the impurities hydrogen and oxygen into InN films.

To study the effect of unintentional impurities and TD densities on the transport properties of InN, films were grown by PAMBE at varying substrate temperatures and In-fluxes according to the In-face InN growth diagram (Fig. 1).[18] The unintentionally incorporated impurities oxygen and hydrogen were evaluated by secondary ion mass spectrometry (SIMS) in a selection of 1.25 μm thick In-face InN films (represented in Fig. 1 by the red and blue circles). The average impurity concentrations reported here were taken from the bulk areas of the SIMS profile. The top 100 nm of the SIMS profiles were removed from the averaging calculation to eliminate measurement artifacts at the sample surfaces.

TD densities were evaluated by performing x-ray diffraction (XRD) ω-scan rocking curves in both on- and off-axis orientations on a series of 1 μm InN films. Full width half maximum (FWHM) values of these rocking curves were then used to calculate the TD densities of the InN films.[19,20] TD densities given here represent the dominant edge-type TDs determined via extrapolation of the square of the XRD FWHMs of different asymmetric reflections (i.e., twist peak-widths) to an inclination angle of 90° and comparison with plan-view transmission electron microscopy. A complete description of our TD density measurements for these InN films is reported elsewhere.[21,22] To observe the effect of TD densities on the transport properties of InN, a twelve sample

[a]Electronic mail: chadsg@engineering.ucsb.edu.

Downloaded 13 Jul 2009 to 128.111.74.121. Redistribution subject to AIP license or copyright; see http://apl.aip.org/apl/copyright.jsp

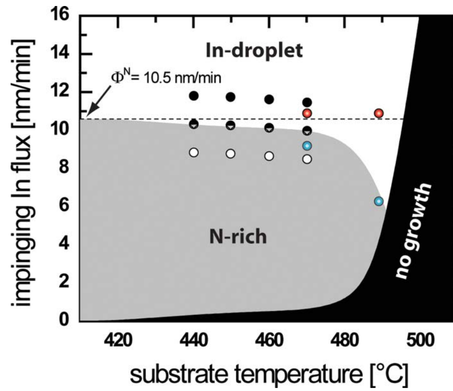

FIG. 1. (Color online) Schematic representation of the In-face InN sample sets used in this study. SIMS analysis was performed on the four samples represented by the colored circles (red for In-droplet growth at 470 and 490 °C and blue for N-rich growth at 470 and 490 °C). XRD analysis was performed to evaluate the TD densities of the samples represented by the remaining circles. Samples were grown at different substrate temperatures varying only the In-flux to establish In-droplet growth conditions (solid black circles), stoichiometric growth conditions (half-filled circles), and N-rich growth conditions (open circles).

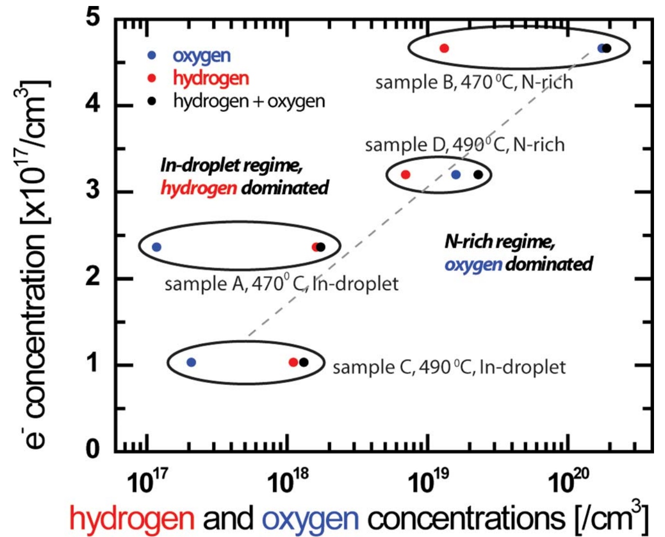

FIG. 2. (Color online) Bulk electron concentration dependence on both hydrogen (red) and oxygen (blue) concentrations for four samples grown under different conditions. The impurity concentrations determined by SIMS measurements scaled closely with the bulk electron concentration.

set was grown at four different substrate temperatures and three different In-fluxes (Fig. 1). The active nitrogen flux was kept constant at growth rate equivalent to $\Phi_N = 10.5$ nm/min. At each substrate temperature the In-fluxes were varied such that growth occurred in the In-droplet regime (solid black circles), the N-rich regime (open circles), and approximately on the stoichiometric crossover from N-rich to In-droplet growth (half-filled circles). Samples grown in the In-droplet regime had an excess impinging In-flux of 2 nm/min and samples grown in the N-rich regime were grown with a deficient In-flux of 2 nm/min.

The transport properties of all the InN films were evaluated by room temperature single-field Hall effect measurements made in the van der Pauw configuration using soldered In contacts. The e^- surface accumulation layer provided a parallel conduction path to the e^- in the bulk film during the Hall effect measurements; therefore, all of the as-measured e^- mobilities and concentrations were a combination of the bulk and surface values. To account for the parallel conduction paths, a two-layer Hall analysis [Eqs. (1) and (2)][23,24] was utilized to calculate the bulk e^- concentrations and mobilities,

$$\mu_{\text{bulk}} = \frac{\mu_{\text{Hall}}^2 n_{\text{Hall}} - \mu_{\text{surface}}^2 n_{\text{surface}}}{\mu_{\text{Hall}} n_{\text{Hall}} - \mu_{\text{surface}} n_{\text{surface}}}, \tag{1}$$

$$n_{\text{bulk}} = \frac{(\mu_{\text{Hall}} n_{\text{Hall}} - \mu_{\text{surface}} n_{\text{surface}})^2}{\mu_{\text{Hall}}^2 n_{\text{Hall}} - \mu_{\text{surface}}^2 n_{\text{surface}}}, \tag{2}$$

where n_{Hall} was the as-measured sheet carrier concentration, μ_{Hall} was the as-measured e^- mobility, n_{Surface} was the experimentally determined, temperature-independent[25,26] surface sheet concentration of 5×10^{13} e^-/cm^2, and μ_{Surface} was the experimentally determined, temperature-independent surface e^- mobility of 500 cm^2/V s.[25,26] It is important to note that the surface e^- concentrations and mobilities were not individually measured for each sample in this study. We calculated the bulk e^- concentrations and mobilities using a range of surface values[25,26] and found the resulting calculated bulk values varied only slightly (+/−5%). For clarity, both the calculated and as-measured values are reported. The trends discussed below are similar for both the as-measured and calculated values.

The SIMS data presented here (Table I) were taken from InN films grown at two different substrate temperatures (470 and 490 °C) in both the In-droplet and N-rich growth regimes. The samples grown with the highest In-fluxes had less observed hydrogen and oxygen than the samples grown N-rich. The samples grown at 490 °C also exhibited lower impurity concentrations relative to the samples grown at 470 °C. The impurity concentrations scaled directly with the carrier concentrations (Fig. 2). The samples exhibiting the highest carrier concentrations had also the highest impurity concentrations. Samples grown in the N-rich regime had particularly high oxygen concentrations as compared to the samples grown with excess In. The lower impurity concentrations in the In-droplet grown films indicated that the In-adlayer present during In-droplet growth[18] suppressed impurity incorporation, most notably oxygen. Higher growth

TABLE I. Summary of SIMS and transport data for the four differently grown samples schematically depicted in Fig. 1 and graphically presented in Fig. 2.

Sample	Growth regime	T_{sub} (°C)	Ave. Oxygen (/cm^3)	Ave. Hydrogen (/cm^3)	Carrier concentration (calc./measured) (electron/cm^3)	Mobility (calc./measured) (cm^2/V s)
A	In-droplet	470	1.18×10^{17}	1.62×10^{18}	$2.37 \times 10^{17}/3.88 \times 10^{17}$	2080/1541
B	N-rich	470	1.76×10^{20}	1.32×10^{19}	$4.66 \times 10^{17}/5.92 \times 10^{17}$	1726/1431
C	In-droplet	490	2.08×10^{17}	1.11×10^{18}	$1.03 \times 10^{17}/8.30 \times 10^{17}$	2749/1685
D	N-rich	490	1.60×10^{19}	7.01×10^{18}	$3.20 \times 10^{17}/5.6 \times 10^{18}$	2085/1647

Downloaded 13 Jul 2009 to 128.111.74.121. Redistribution subject to AIP license or copyright; see http://apl.aip.org/apl/copyright.jsp

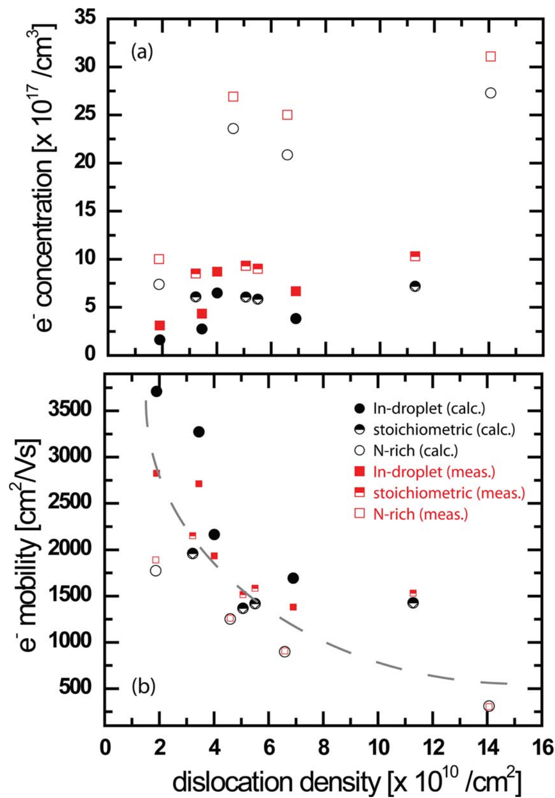

FIG. 3. (Color online) (a) Calculated bulk electron concentration (black) and as-measured electron concentration (red) dependence on TD density. (b) Calculated bulk electron mobility (black) and as-measured electron mobility (red) dependence on TD density.

temperatures also acted as a barrier to impurity incorporation as evidenced by the decrease in average impurity concentrations for samples grown at higher temperatures. It is important to note that growth conditions have little effect on In-vacancy concentration as determined by positron annihilation spectroscopy.[27] The In-vacancy concentrations were below the room temperature detection limit and measured to be only $1-6\times10^{16}$ cm^{-3} at low temperatures for a range of differently grown samples,[27] suggesting these vacancies had negligible effect on the e^- transport properties.

The presence of hydrogen in these films presents a significant problem in controlling the conductivity of InN. Hydrogen is ubiquitous even in ultrahigh vacuum MBE systems and the removal of a significant amount of hydrogen would require unreasonable or unachievable measures. With the recent discovery that hydrogen could actually donate two e^- to the bulk when incorporated on a nitrogen site,[17] the hydrogen problem becomes even more central to limiting the control of conductivity in InN.

No observable dependence of the e^- concentration on TD density was discernable [Fig. 3(a)]. This was particularly evident when considering the samples grown in the In-droplet regime (filled circles/squares) as opposed to samples grown in N-rich conditions (empty circles/squares). The three samples with the lowest TD densities for both In-droplet and N-rich grown films exhibited significantly different carrier concentrations while having similar TD densities. These N-rich InN films had e^- concentrations four to five times higher than samples grown with excess In. The films grown at roughly stoichiometric conditions (partially filled circles/squares) exhibited relatively constant carrier concentrations ($\sim5\times10^{17}$ cm^{-3}) with increasing TD densities (from 3 to 11×10^{10} cm^{-2}). Films grown in the In-droplet regime exhibited the lowest overall TD densities and e^- concentrations and showed little dependence of carrier concentration on TD density. InN films grown in the N-rich regime also exhibited relatively constant e^- concentrations with increasing TD densities. The bulk e^- mobility decreased with TD density when considering the entire data set [Fig. 3(b)], demonstrating that TDs act as dominant e^- scattering centers. A similar dependence can be observed in each series grown using the same In-flux.

[1] L. F. J. Piper, T. D. Veal, C. F. McConville, L. Hai, and W. J. Schaff, Appl. Phys. Lett. **88**, 252109 (2006).
[2] V. Lebedev, V. Cimalla, T. Baumann, O. Ambacher, F. M. Morales, J. G. Lozano, and D. Gonzalez, J. Appl. Phys. **100**, 094903 (2006).
[3] X. Wang, S.-B. Che, Y. Ishitani, and A. Yoshikawa, Appl. Phys. Lett. **90**, 151901 (2007).
[4] D. C. Look, H. Lu, W. J. Schaff, J. Jasinski, and Z. Liliental-Weber, Appl. Phys. Lett. **80**, 258 (2002).
[5] P. J. Hansen, Y. E. Strausser, A. N. Erickson, E. J. Tarsa, P. Kozodoy, E. G. Brazel, J. P. Ibbetson, U. Mishra, V. Narayanamurti, S. P. DenBaars, and J. S. Speck, Appl. Phys. Lett. **72**, 2247 (1998).
[6] J. S. Thakur, R. Naik, V. M. Naik, D. Haddad, G. W. Auner, H. Lu, and W. J. Schaff, J. Appl. Phys. **99**, 023504 (2006).
[7] K. Wang, Y. Cao, J. Simon, J. Zhang, A. Mintairov, J. Merz, D. Hall, T. Kosel, and D. Jena, Appl. Phys. Lett. **89**, 162110 (2006).
[8] K. S. A. Butcher, A. J. Fernandes, P. P. T. Chen, M. Wintrebert-Fouquet, H. Timmers, S. K. Shrestha, H. Hirshy, R. M. Perks, and F. U. Brian, J. Appl. Phys. **101**, 123702 (2007).
[9] J. C. Ho, P. Specht, Q. Yang, X. Xu, D. Hao, and E. R. Weber, J. Appl. Phys. **98**, 093712 (2005).
[10] A. Laakso, J. Oila, A. Kemppinen, K. Saarinen, W. Egger, L. Liszkay, P. Sperr, H. Lu, and W. J. Schaff, J. Cryst. Growth **269**, 41 (2004).
[11] K. S. A. Butcher, M. Wintrebert-Fouquet, P. P. T. Chen, T. L. Tansley, H. Dou, S. K. Shrestha, H. Timmers, M. Kuball, K. E. Prince, and J. E. Bradby, J. Appl. Phys. **95**, 6124 (2004).
[12] C. Stampfl, C. G. Van de Walle, D. Vogel, P. Kruger, and J. Pollmann, Phys. Rev. B **61**, R7846 (2000).
[13] C. S. Gallinat, G. Koblmuller, J. S. Brown, S. Bernardis, J. S. Speck, G. D. Chern, E. D. Readinger, H. Shen, and M. Wraback, Appl. Phys. Lett. **89**, 032109 (2006).
[14] S. Limpijumnong and C. G. Van De Walle, Phys. Status Solidi B **228**, 303 (2001).
[15] C. G. Van de Walle and J. Neugebauer, J. Appl. Phys. **95**, 3851 (2004).
[16] C. G. Van de Walle and J. Neugebauer, Nature (London) **423**, 626 (2003).
[17] A. Janotti and C. G. Van de Walle, Appl. Phys. Lett. **92**, 032104 (2008).
[18] C. S. Gallinat, G. Koblmuller, J. S. Brown, and J. S. Speck, J. Appl. Phys. **102**, 064907 (2007).
[19] S. R. Lee, A. M. West, A. A. Allerman, K. E. Waldrip, D. M. Follstaedt, P. P. Provencio, D. D. Koleske, and C. R. Abernathy, Appl. Phys. Lett. **86**, 241904 (2005).
[20] V. Srikant, J. S. Speck, and D. R. Clarke, J. Appl. Phys. **82**, 4286 (1997).
[21] C. S. Gallinat, G. Koblmuller, F. Wu, and J. S. Speck, "Evaluation of threading dislocation densities in In-face InN," J. Appl. Phys. (unpublished).
[22] C. S. Gallinat, Doctoral dissertation, University of California at Santa Barbara, 2008.
[23] D. C. Look, *Electrical Characterization of GaAs Materials and Devices* (Wiley, New York, 1989).
[24] D. C. Look and R. J. Molnar, Appl. Phys. Lett. **70**, 3377 (1997).
[25] T. Fehlberg, C. Gallinat, G. Umana-Membreno, G. Koblmüller, B. Nener, J. Speck, and G. Parish, J. Electron. Mater. **37**, 593 (2007).
[26] T. B. Fehlberg, G. A. Umana-Membreno, B. D. Nener, G. Parish, C. S. Gallinat, G. Koblmüller, S. Rajan, S. Bernardis, and J. S. Speck, Jpn. J. Appl. Phys., Part 2 **45**, L1090 (2006).
[27] F. Reurings, F. Tuomisto, C. S. Gallinat, G. Koblmüller, and J. S. Speck, Phys. Status Solidi C **6**, S401 (2009).

Downloaded 13 Jul 2009 to 128.111.74.121. Redistribution subject to AIP license or copyright; see http://apl.aip.org/apl/copyright.jsp

In adlayer mediated molecular beam epitaxial growth and properties of *a*-plane InN on freestanding GaN

G. Koblmüller,[1,a)] G. D. Metcalfe,[2] M. Wraback,[2] F. Wu,[1] C. S. Gallinat,[1] and J. S. Speck[1]
[1]*Materials Department, University of California, Santa Barbara, California 93106, USA*
[2]*Sensors and Electron Devices Directorate, U.S. Army Research Laboratory, Maryland 20783, USA*

(Received 4 February 2009; accepted 5 February 2009; published online 4 March 2009)

The role of the In adlayer on the morphological and structural properties of nonpolar *a*-plane InN films was elucidated during the plasma-assisted molecular beam epitaxy on freestanding GaN. Reflection high energy electron diffraction during In adsorption experiments on *a*-plane InN surfaces revealed a stable In adlayer coverage of ~2 ML. This In adlayer-mediated growth was responsible for achieving atomically smooth surfaces (rms roughness of <1 nm), phase-pure material with lower x-ray rocking curve widths ($\Delta\omega < 0.5°$), lower crystal mosaic tilt/twist, and decreased stacking fault densities, compared to N-rich conditions. The photoluminescence peak emission and band gap energy of the *a*-plane InN films were ~0.63 and ~0.7 eV, respectively. © *2009 American Institute of Physics*. [DOI: 10.1063/1.3092482]

Despite intense efforts to enhance many physical properties of indium nitride (InN), this underdeveloped group-III nitride material has found relatively few applications in devices. These limitations are in part caused by an electron accumulation layer at the InN surface due to surface Fermi level pinning in the conduction band,[1] restricting the fabrication of *p*-type InN layers.[2] To facilitate pure *p*-type InN and drive research toward device applications, first-principle calculations[3] suggested that growth along nonpolar, i.e., the *a*-plane ($[11\bar{2}0]$) and *m*-plane ($[1\bar{1}00]$) orientations, would yield surfaces without an accumulation layer. However, this was proposed only for reconstructed nonpolar InN surfaces without metal adlayers or In–In bonding states in the conduction band. The absence of electron accumulation on nonpolar InN surfaces was recently demonstrated, indeed, on *in situ* cleaved *a*-plane InN,[4] but not on as-grown surfaces, due to nonhomogeneous, highly defective surfaces[5,6] and metal In coverage,[7] which contributed to *n*-type surface states in both *a*- and *m*-plane InN.

So far, all *a*-plane InN films were grown on *r*-plane ($[1\bar{1}02]$) sapphire, which suffered from cubic inclusions,[8] three-dimensional (3D) growth mode,[5] surface roughness >50 nm (Ref. 9) and poor electronic transport (electron mobilities at <250 cm^2/V s),[5] pointing to apparent difficulties in fabricating high-quality nonpolar InN. More recently though, the first step toward phase-pure nonpolar InN films with smooth surfaces was achieved for the *m*-plane, owing to the availability of high-quality freestanding *m*-plane GaN substrates and knowledge of thermal dissociation.[10]

To establish *a*-plane InN films with similar qualities and understand the critical In adlayer issues, we report in this letter on the influence of the In adlayer kinetics during the plasma-assisted molecular beam epitaxy (PAMBE) on the surface and structural properties of the *a*-plane InN. Specifically, under In-rich conditions, In-adlayer-mediated growth was found to enhance the surface diffusion, the film mosaic, and the basal-plane stacking fault densities, surpassing previous problems associated with *a*-plane InN films.

As substrate material, on-axis *a*-plane freestanding GaN (Mitsubishi Chemical Co.) was used, which was sliced from a bulk GaN crystal along its *c*-direction. The *a*-plane InN films were grown in a Varian Gen-II MBE system, equipped with standard effusion cells for In and Ga. Active nitrogen was supplied by a Veeco Unibulb radio-frequency plasma source, using a N_2 flow rate of 0.4 sccm and plasma power of 300 W (i.e., equivalent to N limited growth rate of ~6 nm/min). To produce low-impurity InN/GaN interfaces, the *a*-plane GaN substrates were overgrown with ~50 nm of MBE-GaN under Ga-rich conditions.

First, the onset for thermal dissociation was determined by recording the reflection high-energy electron diffraction (RHEED) intensity during the growth of ~10 min long InN pulses under variable temperatures ($T = 380-500$ °C) at constant N-rich conditions (In/N=0.8).[10] As typical for N-rich group-III nitride growth,[11] these pulses produced spotty RHEED patterns, however, only up to $T \sim 430$ °C. Higher temperatures resulted in very low-contrast RHEED patterns due to the large In droplets accumulating on the surface as a result of thermal dissociation.[12] Thus, ~430 °C was the practical onset temperature for thermal dissociation, being nearly identical to that for *m*-plane InN,[10] but much lower than the dissociation temperature reported for *c*-plane InN.[13,14]

We selected therefore $T = 420$ °C as the maximum growth temperature and further analyzed the effect of the In/N flux ratio on the surface morphology. The atomic force micrographs in Fig. 1 show surfaces of three *a*-plane InN films grown under different In/N flux ratios, i.e., (a)=0.6 (N-rich growth), (b)=1 (flux stoichiometry), and (c)=1.25 (In-rich growth). The film thicknesses varied between (a)

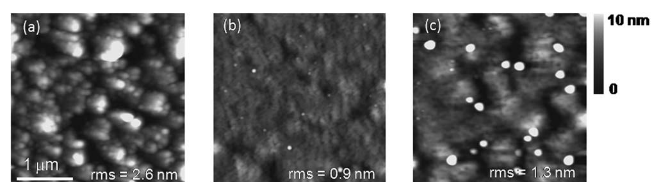

FIG. 1. 3×3 μm^2 AFM images of *a*-plane InN grown on freestanding GaN at constant $T = 420$ °C, but variable In/N flux ratio: (a) In/N=0.6, (b) In/N=1, and (c) In/N=1.25.

a)Author to whom correspondence should be addressed. Electronic mail: Gregor.Koblmueller@wsi.tum.de.

 © 2009 American Institute of Physics

Downloaded 05 Mar 2009 to 128.111.193.10. Redistribution subject to AIP license or copyright; see http://apl.aip.org/apl/copyright.jsp

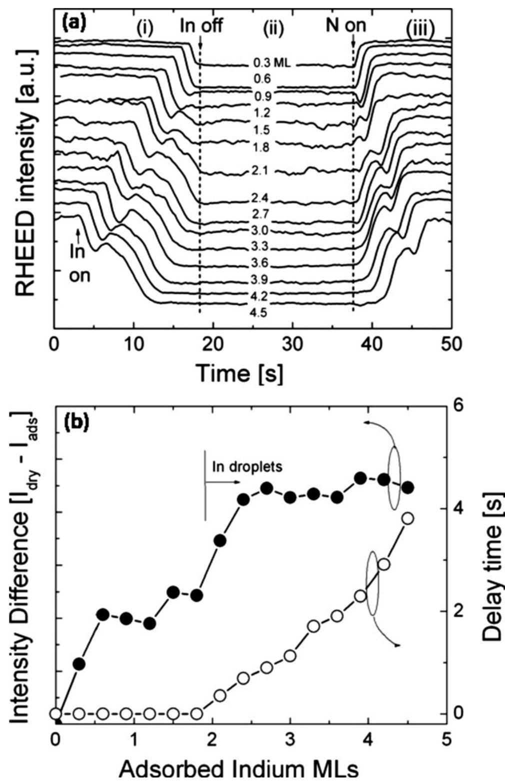

FIG. 2. (a) RHEED intensity profiles during the adsorption of different In coverages and their consecutive consumption by active N on *a*-plane InN surfaces. Note that pronounced oscillatory transients indicated a saturated In-adlayer coverage of 2 ML. (b) Further evidence of the 2 ML thick In-adlayer shown by the saturation in RHEED intensity difference (determined from intensity levels between nitridated and In-adlayer-stabilized surfaces) and the In-droplet related delay in the oscillation onset for In > 2 ML.

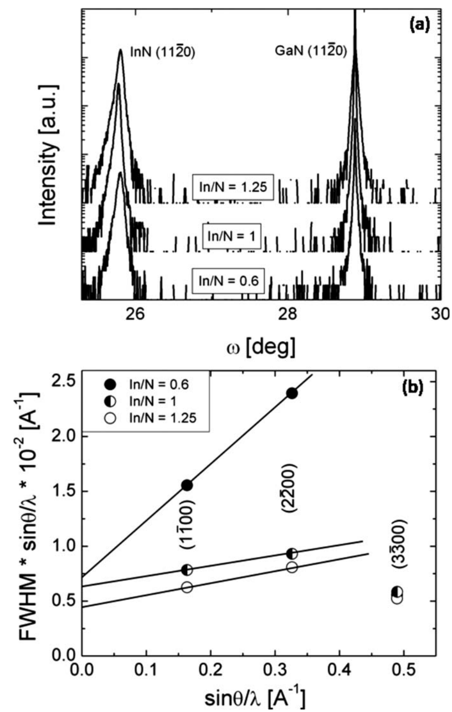

FIG. 3. (a) ω-2θ XRD scans of *a*-plane InN films grown on *a*-plane free-standing GaN under different In/N flux ratios (0.6–1.25). (b) WH plots of the BPSF sensitive reflections in the *m*-plane scattering plane and in skew symmetry for the same three InN films, giving the mosaic tilt/twist by the fitted slope angles and the BPSF density from the intercept with the ordinate.

300 nm, (b) 900 nm, and (c) 500 nm, respectively. Obviously, N-rich conditions yielded highly facetted 3D surfaces with rms ~2.6 nm (over 3×3 μm^2). Crossing flux stoichiometry toward more In-rich conditions reduced the 3D features and decreased the rms roughness to ~1 nm. The dots visible in Fig. 3(c) represent In droplets.

M-plane InN surfaces showed striated morphologies along the *a*-direction that were associated with the intersection of basal plane stacking faults with the surface.[10,15–17] Such striations were absent on the *a*-plane InN surfaces, as was the case for *a*-plane GaN.[18] This low morphological anisotropy could be attributed to similar adatom diffusion energies along the in-plane *c*- and *m*-directions on *a*-plane surfaces, compared to the more different energies along the *c*- and *a*-directions calculated for *m*-plane surfaces.[19]

To explain the much smoother morphologies for films grown above flux stoichiometry ($In/N\geq1$), we proposed a stable In adlayer at the growth surface that enhances the surface diffusion. This In adlayer and its maximum coverage on the *a*-plane InN was identified via specific RHEED intensity measurements. By adsorbing variable In coverages (0.3–4.5 ML) onto a nitridated InN surface and subsequently consuming these by InN growth with active nitrogen (all at a fixed $T=400$ °C), various different RHEED intensity curves were observed [Fig. 2(a)]. Note that 1 ML of In corresponds to the unit cell height of the *a*-plane InN, i.e., $a^{InN}/2=1.77$ Å.

Three different regimes were characterized: (i) drop in intensity upon In adsorption due to the formation of the In adlayer, (ii) constant intensity after closing the In shutter (In-adlayer stabilized surface), and (iii) rise in intensity during the consumption of the In adlayer by an active N, resulting in the initially nitridated surface. Also, with increasing In adsorption time (duration between "In on" and "In off") different oscillatory transients were observed, depending on the amount of adsorbed In. For In coverages below 1 ML, barely any oscillatory transients were found, while for 1 ML < In < 2 ML, clear oscillatory transients appeared.

For In coverages >2 ML there was a gradual delay in the onset of the oscillatory transient upon N consumption [Fig. 2(b)], indicating that In droplets formed. In addition, plotting the difference in the RHEED intensity between the fully nitridated and In-adlayer stabilized surface, we observed a steady increase with rising In coverage until saturation occurred for In coverages of ≥2 ML [Fig. 2(b)]. From all these observations we can clearly state that the maximum In adlayer coverage on *a*-plane InN amounts to ~2 ML, similar to the reported In adlayer coverage on *c*-plane InN.[20]

The role of the In adlayer on the structural properties was analyzed by high-resolution x-ray diffraction, shown by

TABLE I. Measured values of XRD rocking curve widths from (11$\bar{2}$0) ω scans along both the in-plane *c*- and *m*-orientations; the corresponding film mosaic tilt/twist $\Delta\omega$ (skew) and BPSF densities from WH analysis for the three investigated *a*-plane InN films.

	$\Delta\omega(11\bar{2}0)$			
In/N	*m* (deg)	*c* (deg)	$\Delta\omega$ (skew) (deg)	ρ (SF) (cm^{-1})
0.6	0.62	0.68	2.94	1.5×10^6
1	0.54	0.63	0.51	1.2×10^6
1.25	0.49	0.56	0.64	8.8×10^5

Downloaded 05 Mar 2009 to 128.111.193.10. Redistribution subject to AIP license or copyright; see http://apl.aip.org/apl/copyright.jsp

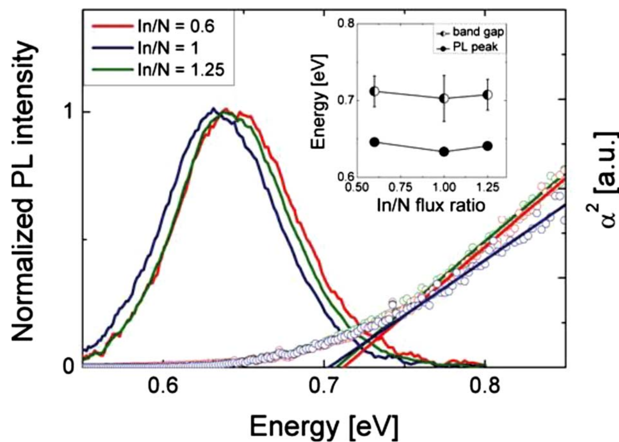

FIG. 4. (Color online) Room temperature PL and optical absorption spectra for the three selected *a*-plane InN films grown at $T=420$ °C and varying In/N flux ratios. The band gap energy was determined by the intercept of the linear fits of the square of the absorption coefficient with the energy axis.

the $(11\bar{2}0)$ ω-2θ scans of the three *a*-plane InN films grown under the different In/N flux ratios in Fig. 3(a). For all films, two single diffraction peaks were identified, associated with the *a*-plane InN film and the *a*-plane GaN substrate. We also measured the $(11\bar{2}0)$ rocking curve widths [full width at half maximum (FWHM) of ω scans] for the two orthogonal in-plane *c*-([0001]) and *m*-($[1\bar{1}00]$) orientations, as listed in Table I. Two main trends were found: (i) A gradual decrease in FWHMs with increasing In/N flux ratio for both orientations, and (ii) slightly lower FWHMs along the *m*-orientation, although this deviation was not too significant due to the similar adatom diffusion[19] and low morphological anisotropy along the two orthogonal in-plane orientations.

The FWHMs of ω scans contain contributions by the basal-plane stacking faults (BPSFs), which can be separated by Williamson–Hall (WH) analysis.[21,22] However, both the accessible on-axis reflections of the *a*-plane InN, i.e., $(11\bar{2}0)$ and $(22\bar{4}0)$, were found insensitive to the BPSFs and the derived FWHMs would yield only the mosaic tilt.[23,24] Determining the BPSFs, we focused on the BPSF sensitive reflections $(1\bar{1}00)$ and $(2\bar{2}00)$ (within the *m*-scattering plane), being readily accessible in skew symmetry ($\psi=30°$).[24]

The FWHMs of these BPSF sensitive reflections $(1\bar{1}00)$ and $(2\bar{2}00)$ are shown in the WH plot in Fig. 3(b) together with the insensitive reflections $(3\bar{3}00)$ for the three *a*-plane InN films. In skew geometry both tilt and twist mosaics contribute to the broadening of the XRD ω scans, meaning they are contained in the derived slope angles $\Delta\omega$ (skew), while the intercept with the ordinate yielded the BPSF density for each sample. Summarized in Table I, we noted a drastic reduction in film mosaic tilt/twist (from ~3° to ~0.5°) and a decrease in BPSF densities (from $\sim 1.5\times 10^6$ to $\sim 8\times 10^5$ cm^{-1}) for the crossover from N-rich to In-rich growth. These values were also confirmed by transmission electron microscopy, highlighting the powerful nondestructive approach of the WH analysis.

Finally, the band gap energy was analyzed by photoluminescence (PL) and optical absorption at 300 K (Fig. 4). PL peak emission and band gap energies were independent of In/N ratio with values between 0.632–0.645 eV and $(0.70-0.71)\pm 0.03$ eV, respectively. The ~70 meV redshift of the PL peak with respect to the band gap energy was comparable to that for the *m*-plane InN,[10] but larger than the typical Stokes shift of ~20–25 meV in *c*-plane InN.[13,14] This may be associated with the increased numbers of band-tail states in nonpolar InN due to the decoration of BPSFs by large point defect densities, mainly impurities.[25] The PL and band gap data are in good agreement with previous reports of *a*-plane InN (Refs. 5 and 26) and *c*-plane InN.[1,13,14]

The authors would like to thank C. Van de Walle for fruitful discussions and A. Hirai for the support with XRD analysis. This work was supported by AFOSR (D. J. Silversmith, program manager) and performed at the MRSEC facilities at UCSB (supported by NSF).

[1] H. Lu, W. J. Schaff, L. F. Eastman, J. Wu, W. Walukiewicz, V. Cimalla, and O. Ambacher, Appl. Phys. Lett. **82**, 1736 (2003).
[2] P. A. Anderson, C. H. Swartz, D. Carder, R. J. Reeves, S. M. Durbin, S. Chandril, and T. H. Myers, Appl. Phys. Lett. **89**, 184104 (2006).
[3] D. Segev and C. G. Van de Walle, Europhys. Lett. **76**, 305 (2006).
[4] C. L. Wu, H. M. Lee, C. T. Kuo, C. H. Chen, and S. Gwo, Phys. Rev. Lett. **101**, 106803 (2008).
[5] H. Lu, W. J. Schaff, L. F. Eastman, J. Wu, W. Walukiewicz, V. Cimalla, and O. Ambacher, Appl. Phys. Lett. **83**, 1136 (2003).
[6] P. D. C. King, T. D. Veal, C. F. McConville, F. Fuchs, J. Furthmüller, F. Bechstedt, P. Schley, R. Goldhahn, J. Schörmann, D. J. As, K. Lischka, D. Muto, H. Naoi, Y. Nanishi, H. Lu, and W. J. Schaff, Appl. Phys. Lett. **91**, 092101 (2007).
[7] E. Calleja, J. Grandal, M. A. Sanchez–Garcia, M. Niebelschütz, V. Cimalla, and O. Ambacher, Appl. Phys. Lett. **90**, 262110 (2007).
[8] Y. Kumagai, A. Tsuyuguchi, H. Naoi, T. Araki, H. Na, and Y. Nanishi, Phys. Status Solidi B **243**, 1468 (2006).
[9] X. L. Zhu, L. W. Guo, M. Z. Peng, B. H. Ge, J. Zhang, G. J. Ding, H. Q. Jia, H. Chen, and J. M. Zhou, J. Cryst. Growth **310**, 3726 (2008).
[10] G. Koblmüller, A. Hirai, F. Wu, C. S. Gallinat, G. D. Metcalfe, H. Shen, M. Wraback, and J. S. Speck, Appl. Phys. Lett. **93**, 171902 (2008).
[11] H. Okumura, K. Balakrishnan, H. Hamaguchi, T. Koizumi, S. Chichibu, H. Nakanishi, T. Nagatomo, and S. Yoshida, J. Cryst. Growth **189**, 364 (1998).
[12] G. Koblmüller, C. S. Gallinat, and J. S. Speck, J. Appl. Phys. **101**, 083516 (2007).
[13] C. S. Gallinat, G. Koblmüller, J. S. Brown, S. Bernardis, J. S. Speck, G. D. Chern, E. D. Readinger, H. Shen, and M. Wraback, Appl. Phys. Lett. **89**, 032109 (2006).
[14] G. Koblmüller, C. S. Gallinat, S. Bernardis, J. S. Speck, G. D. Chern, E. D. Readinger, H. Shen, and M. Wraback, Appl. Phys. Lett. **89**, 071902 (2006).
[15] B. A. Haskell, A. Chakraborty, H. Sasano, P. T. Fini, S. P. DenBaars, J. S. Speck, and S. Nakamura, J. Electron. Mater. **34**, 357 (2005).
[16] M. McLaurin, T. E. Mates, F. Wu, and J. S. Speck, J. Appl. Phys. **100**, 063707 (2006).
[17] A. Hirai, B. A. Haskell, M. B. McLaurin, F. Wu, M. C. Schmidt, K. C. Kim, T. J. Baker, S. P. DenBaars, S. Nakamura, and J. S. Speck, Appl. Phys. Lett. **90**, 121119 (2007).
[18] M. D. Craven, S. H. Lim, F. Wu, J. S. Speck, and S. P. DenBaars, Appl. Phys. Lett. **81**, 469 (2002).
[19] L. Lymperakis and J. Neugebauer, Proceedings of the International Workshop on Nitride Semiconductors, Montreux, 2008 (unpublished).
[20] C. S. Gallinat, G. Koblmüller, and J. S. Speck, J. Appl. Phys. **102**, 064907 (2007).
[21] T. Metzger, R. Höpler, E. Born, O. Ambacher, M. Stutzmann, R. Stömmer, M. Schuster, H. Göbel, S. Christiansen, M. Albrecht, and H. P. Strunk, Philos. Mag. A **77**, 1013 (1998).
[22] M. B. McLaurin, A. Hirai, E. Young, F. Wu, and J. S. Speck, Jpn. J. Appl. Phys. **47**, 5429 (2008).
[23] M. D. Craven, F. Wu, A. Chakraborty, B. Imer, S. P. DenBaars, and J. S. Speck, Appl. Phys. Lett. **84**, 1281 (2004).
[24] A. Hirai, F. Wu, and J. S. Speck (unpublished).
[25] P. Paskov, R. Schifano, B. Monemar, T. Paskova, S. Figge, and H. Hommel, J. Appl. Phys. **98**, 093519 (2005).
[26] F. Shikata, S. Hirano, T. Inoue, M. Orihara, Y. Hijikata, H. Yaguchi, and S. Yoshida, J. Cryst. Growth **301**, 517 (2007).

Downloaded 05 Mar 2009 to 128.111.193.10. Redistribution subject to AIP license or copyright; see http://apl.aip.org/apl/copyright.jsp

Growth of high quality N-polar AlN(000$\bar{1}$) on Si(111) by plasma assisted molecular beam epitaxy

Sansaptak Dasgupta,[1,a)] F. Wu,[2] J. S. Speck,[2] and U. K. Mishra[1]
[1]*Department of Electrical and Computer Engineering, University of California, Santa Barbara, California 93106, USA*
[2]*Department of Materials, University of California, Santa Barbara, California 93106, USA*

(Received 27 December 2008; accepted 24 March 2009; published online 14 April 2009)

High quality N-polar AlN epilayers were grown and characterized on Si(111) substrates by plasma assisted molecular beam epitaxy as a first step toward growth of N-polar nitrides on Si(111). Polarity inversion to N-face by an optimized predeposition of Al adatoms on the reconstructed 7×7 Si(111) surface was investigated. Al adatoms can saturate the dangling bonds of Si atoms, resulting in growth of AlN in (000$\bar{1}$) direction on subsequent exposure to N_2 plasma. N-polarity was confirmed by observing strong 3×3 and 6×6 reflection high-energy electron diffraction reconstructions, convergent beam electron diffraction imaging and KOH etching studies. The structural properties were investigated by x-ray diffraction measurements, cross section and plan-view TEM studies. © *2009 American Institute of Physics*. [DOI: 10.1063/1.3118593]

In nitride technology silicon substrates offer several advantages compared to SiC and sapphire, such as lower cost, good electrical conductivity, larger wafers, and the possibility of integration of nitrides with the existing Si technologies. Despite the fact that heteroepitaxy of nitrides on Si(111) suffers from large lattice mismatch [19% for AlN on Si(111)] and differences in thermal expansion coefficients, the growth of high quality nitrides on Si(111) substrates has shown a marked improvement in recent years, leading to fabrication of electronic devices.[1–3] Growth of high quality GaN on large area Si substrates has also been demonstrated by metal-organic vapor phase epitaxy[4] and metal-organic chemical vapor deposition.[5]

Conventionally, Ga-polar nitride-based devices have demonstrated excellent high power and high frequency performance[6,7] while N-polar devices have been less investigated.[8] However, N-polar heterostructures are particularly attractive for enhancement mode devices, highly scaled submicron transistors, and for the fabrication of nitride-based solar cells. Reports on growth and characterization of N-polar nitrides on Si(111) are limited and most growth studies and characterization have been performed on metal-polar nitrides on Si(111).[9] The technique used to grow N-polar nitrides is mostly substrate nitridation to form a layer of SiN_x prior to the growth of the nitride.[10] However the formation of crystalline SiN_x is extremely difficult and amorphous SiN_x layers are formed at the onset of the nitride growth. This affects the structural quality of the epilayer and its crystallinity. The mechanism of the polarity inversion is also poorly understood.

The adsorption of group III adatoms on Si(111) and its different phases and structures have been studied in great detail.[11] Al adatoms deposited on a 7×7 reconstructed Si(111) surface have been shown to occupy the H_3 (hollow) as well as T_4 (atop) sites. These distinguish the two cases when the substrate atom (Si) below the Al adatom is found in the fourth (H_3) or in the second layer (T_4). Accurate deposition of Al monolayers can then lead to the formation of the Al/Si(111) γ phase, where the Al adatom saturates the underlying dangling bonds of Si, as demonstrated by Yasutake *et al.*[12] Subsequent exposure to N_2 plasma would then suggest a N-polar growth orientation, where the N atoms can bond with the empty p_z orbital of the Al atoms (Fig. 1).

In this paper, we explore the growth and structural characterization of N-polar AlN on Si(111) by plasma assisted molecular beam epitaxy (PAMBE), using adequate predeposition of Al adatoms on Si(111) surface as a technique to invert polarity. The structural quality of the films was evaluated by x-ray diffraction (XRD) studies and transmission electron microscopy (TEM). By optimizing the amount of Al predeposition prior to AlN growth we were able to obtain films with uniform N-polarity. Different growth temperatures for the AlN film were also explored to optimize the surface morphology and structural properties.

The samples for this study were grown in a Varian Gen II MBE system equipped with an AppliedEpi Unibulb rf-plasma source for active nitrogen. Ultrahigh purity nitrogen (99.9995% pure) was further purified by an inert gas purifier. In all the experiments, the N_2 flow rate was kept constant at 0.3 SCCM (SCCM denotes cubic centimeter per minute at STP) and the plasma power was 250 W. The growth rate was

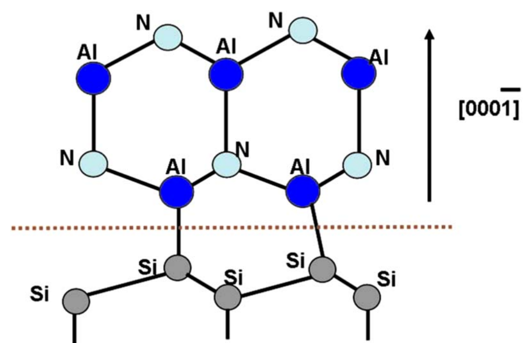

FIG. 1. (Color online) Schematic of possible bonding configuration of Al at the Al/Si(111) interface. The Al adatoms saturate the Si dangling bonds, and subsequent exposure to N* plasma results in a [000$\bar{1}$] growth direction.

a)Electronic mail: sansaptak@ece.ucsb.edu.

 © 2009 American Institute of Physics

Downloaded 14 Apr 2009 to 128.111.193.10. Redistribution subject to AIP license or copyright; see http://apl.aip.org/apl/copyright.jsp

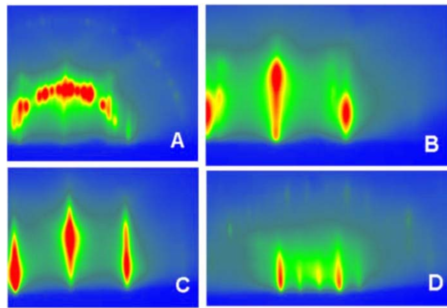

FIG. 2. (Color online) RHEED evolution during the growth viewed along the $\langle 11\bar{2}0\rangle$ direction. (a) 7×7 reconstructions of the clean Si(111) surface after oxide desorption. (b) After 12 s Al deposition on the reconstructed Si(111) surface. (c) Streaky RHEED pattern during AlN epilayer growth. (d) Strong 3×3 reconstructions indicating N-polarity observed after cooling sample postgrowth below 350 °C.

calibrated to 225 nm/hr by growing GaN/AlGaN heterostructures. Prior to loading in the chamber, Si(111) substrates were ultrasonically cleaned in acetone, methanol and isopropanol. The substrates were then degassed for 2 h at 600 °C before being transferred to the growth chamber. Si(111) substrates were then heated up to 900 °C to desorb the native oxide. Temperatures were monitored by an infrared pyrometer.

At this step, we grew three samples (A, B, and C) with three different Al predeposition time before commencing AlN growth. For this experiment, the growth temperature was fixed at 780 °C throughout the Al predeposition and subsequent AlN growth. Al deposition rate was calibrated based on growth rate calculations for AlN, assuming $c_{AlN}/2$ ($c_{AlN}=0.4982$ nm) for the as-deposited Al. For sample A, we opened the Al shutter for 3 s (which corresponds to 0.75 ML growth of AlN) before opening the N_2 plasma shutter; for sample B, the Al shutter was opened for 12 s (corresponding to 3 ML of AlN) and for sample C, 30 s (corresponding to 7.5 ML of AlN). After the predeposition of Al, 150 nm of AlN was grown for all three samples.

The influence of the growth temperature on the 150 nm thick AlN layers was explored next and additional samples were grown at three different growth temperatures of 775, 800, and 825 °C. For all these samples, a predeposition of 12 s of Al was used to obtain N-polar AlN.

In situ reflection high-energy electron diffraction (RHEED) reconstructions and KOH etching studies were used to study the polarity of the as-grown samples. The surface morphology of the as-grown films were analyzed by atomic force microscopy (AFM), using a Digital Instruments Dimension 3100 instrument operated in tapping mode. The structural properties of the as-grown AlN films were analyzed by XRD measurements using a Philips Material Research X Ray Diffractometer, through rocking curve ω scans around the AlN(0002), AlN($10\bar{1}2$), and AlN($20\bar{2}1$) reflections; the latter two taken in skew geometry (surface normal tilted away from the diffraction plane). The microstructure of the samples was further evaluated by TEM and $[1\bar{1}00]$ zone axis convergent beam electron diffraction (CBED) patterns were recorded with a beam spot size of approximately 40 nm to confirm the N-polarity.

The RHEED patterns at different stages of the growth are shown in Fig. 2. After desorbing the native oxide, and

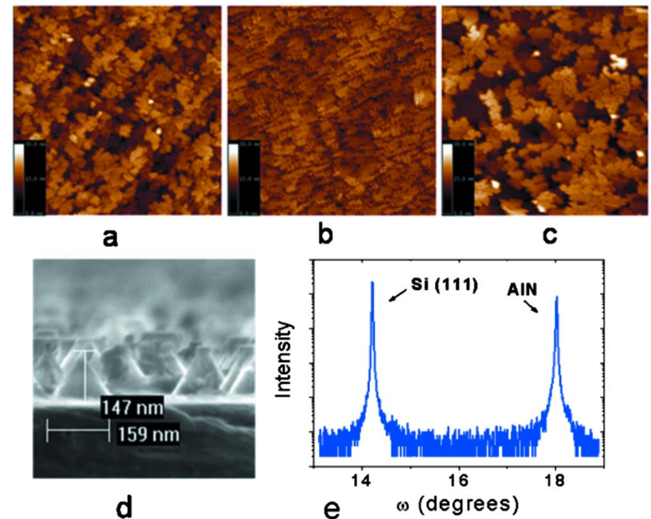

FIG. 3. (Color online) 2×2 μm^2 AFM scans of 150 nm of AlN grown at (a) 775 °C, (b) 800 °C, and (c) 825 °C. (The height scale is 30 nm.) (d) Cross-section scanning electron microscope scan of AlN after KOH etch showing the presence of triangular pyramidal structures. (e) (0002) reflection ω-2θ XRD scan showing the Si(111) and AlN peaks.

cooling down to 700–750 °C clear 7×7 reconstructions characteristic of a clean Si(111) surface was observed [Fig. 2(a)]. Figure 2(b) shows the RHEED image obtained after >3 ML deposition of Al on the 7×7 reconstructed Si(111) surface (samples B and C). This image closely resembles the RHEED pattern for the Al/Si(111) γ phase observed by Yasutake *et al.*[12] We observed streaky RHEED patterns throughout during the subsequent AlN film growth indicating a smooth two-dimensional (2D) epitaxial growth mode [Fig. 2(c)]. For samples B and C, RHEED oscillations with a time period commensurate to the growth rate were also observed. At the end of growth, rapid cooling down to observe surface reconstructions revealed clear 3×3 reconstructions [Fig. 2(d)] at around a temperature of 350 °C and below for only samples B and C, which are indicative of a N-polar film.[13] For sample A, we observed no clear surface reconstructions.

Figure 3 illustrates the different surface morphologies observed at different growth temperatures for the 150 nm AlN films. The rms roughness, for 2×2 μm^2 scans, obtained for the samples grown at 775, 800, and 825 °C were 2.9, 1.6, and 3.5 nm, respectively. We observe a strong dependence of surface morphology on the growth temperature. The sample grown at 800 °C shows a good coalescence of 2D plateletlike structures and a much smoother surface morphology. The relative density of pits and trenches are also drastically reduced in the sample grown at 800 °C. It is to be noted that for all the samples we did not observe any hexagonal islands characteristic of inversion domains, both under the optical microscope and AFM scans. Figure 3(d) shows a cross sectional scanning electron microscopy scan of N-polar AlN grown at 800 °C after etching in 45% KOH solution for 2 min at 80 °C. The surface is vigorously etched, and forms triangular shaped pyramids confirming the N-polarity of the as grown samples.[14]

Rocking curve x-ray scans were performed to record the full width at half maximum (FWHM) values of the (0002), ($10\bar{1}2$), and ($20\bar{2}1$) reflections. These ω scans have been shown to yield estimates for dislocation densities in good agreement with plan-view transmission electron microscope

Downloaded 14 Apr 2009 to 128.111.193.10. Redistribution subject to AIP license or copyright; see http://apl.aip.org/apl/copyright.jsp

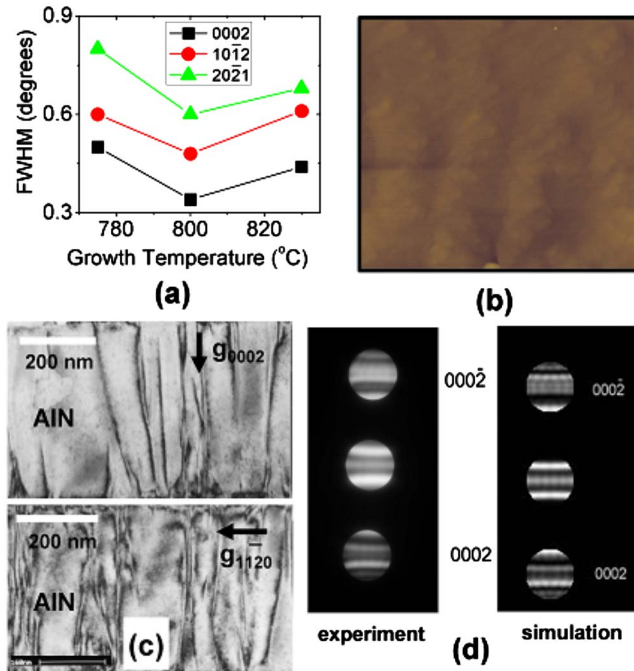

FIG. 4. (Color online) (a) FWHM values obtained from x-ray rocking curve ω scans plotted against the growth temperature of the samples. (b) 5×5 μm^2 AFM scan of 250 nm N-polar AlN grown under optimized conditions showing smooth morphology. (c) Bright field TEM diffraction images of N-polar AlN on Si(111), $g=[0002]$ and $g=[11\bar{2}0]$. (d) Experimental and simulated CBED patterns showing N-polarity of the AlN films.

measurements.[15,16] The on-axis reflection is only sensitive to screw component threading dislocations (TDs) whereas with increasing skew angle the rocking curve widths are primarily affected by edge component TDs. Figure 4(a) shows the different FWHM values obtained through rocking curve XRD scans with respect to growth temperature. The lowest FWHM values for both on-axis and off-axis reflection was obtained for the sample grown at 800 °C. ω-2θ X-ray scans showed the presence of single phase wurtzite AlN on Si(111) and no cubic phases were observed.

Having thus optimized the growth temperature for the AlN(000$\bar{1}$) films, we grew a thicker AlN film of 250 nm on Si(111) using similar predeposition and growth conditions. XRD measurements on this sample yielded FWHM values of 0.3°, 0.38°, and 0.45° for the (0002), (10$\bar{1}$2), and (20$\bar{2}$1) reflections, respectively. 5×5 μm^2 AFM scan of the 250 nm thick N-polar AlN shows rms roughness of 0.4 nm [Fig. 4(b)]. These values indicate excellent structural quality and a good starting point for epitaxial growth of device layers for N-polar heterostructures devices.

The microstructure of the above sample was further examined using TEM and CBED imaging [Fig. 4(c)]. CBED pattern taken from the same sample was compared to the simulated pattern and it confirmed that the AlN layer was N-polar [Fig. 4(d)]. The TD density was estimated to be 2×10^{10} cm^{-2} from plan-view TEM measurements. These values of dislocation density are quite comparable to the dislocation densities obtained for Ga-polar and N-polar GaN grown on SiC by PAMBE.

In summary, we have investigated an approach in obtaining uniform N-polar AlN thick films on Si(111). Through optimized Al deposition prior to growth of AlN, AlN films oriented in the [000$\bar{1}$] direction with smooth surface morphology and superior structural quality were obtained. Growth of N-polar AlN on Si(111) is a first step toward growth of N-polar (Al, Ga, and In) nitride heterostructures on Si(111) for both electronic and photonic device applications. Detailed studies on the improvement of crystal quality and growth of other epitaxial layers and heterostructures are being currently investigated.

The authors would like to thank S. Rajan and S. Keller for useful discussions. The authors gratefully acknowledge financial support from AFOSR and INTEL.

[1]F. Semond, P. Lorenzini, N. Grandjean, and J. Massies, Appl. Phys. Lett. **78**, 335 (2001).
[2]P. Javorka, A. Alam, M. Wolter, A. Fox, H. Luth, and P. Kordos, IEEE Electron Device Lett. **23**, 4 (2002).
[3]A. Krost and A. Dadgar, Mater. Sci. Eng., B **93**, 77 (2002).
[4]K. Cheng, M. Leys, S. Degroote, J. Derluyn, B. Sijmus, P. Favia, O. Richard, H. Bender, M. Germain, and G. Borghs, Jpn. J. Appl. Phys. **47**, 1553 (2008).
[5]A. Ubukata, K. Ikenaga, N. Akutsu, A. Yamaguchi, K. Matsumoto, T. Yamazaki, and T. Egawa, J. Cryst. Growth **298**, 198 (2007).
[6]T. Palacios, A. Chakraborty, S. Heikman, S. Keller, S. P. Denbaars, and U. Mishra, IEEE Electron Device Lett. **27**, 13 (2006).
[7]Y. F. Wu, A. Saxler, A. Moore, R. P. Smith, S. Sheppard, P. M. Chavarkar, T. Wisleder, U. K. Mishra, and P. Parikh, IEEE Electron Device Lett. **25**, 117 (2004).
[8]S. Rajan, A. Chini, M. H. Wong, J. S. Speck, and U. K. Mishra, J. Appl. Phys. **102**, 044501 (2007).
[9]F. Semond, B. Damilano, S. Vezian, N. Grandjean, M. Leroux, and J. Massies, Appl. Phys. Lett. **75**, 82 (1999).
[10]Z. T. Wang and Y. Yamada Takamura, Appl. Phys. Lett. **87**, 032110 (2005).
[11]W. Monch, *Semiconductor Surfaces and Interfaces*, 3rd ed. (Springer, Berlin, 2001), Chap. 15.
[12]K. Yasutake, A. Takeuchi, H. Kakiuchi, and K. Yoshi, J. Vac. Sci. Technol. A **16**, 2140 (1998).
[13]A. Smith, R. M. Feenstra, D. W. Greve, M. S. Shin, M. Skowronksi, J. Neugebauer, and J. E. Northrup, Appl. Phys. Lett. **72**, 2114 (1998).
[14]D. Zhuang and J. H. Edgar, Mater. Sci. Eng. R. **48**, 1 (2005).
[15]V. Srikant, J. Speck, and D. R. Clarke, J. Appl. Phys. **82**, 4286 (1997).
[16]R. Chierchia, T. Bottcher, H. Heinke, S. Enfeldt, S. Figge, and D. Hommel, J. Appl. Phys. **93**, 8918 (2003).

Downloaded 14 Apr 2009 to 128.111.193.10. Redistribution subject to AIP license or copyright; see http://apl.aip.org/apl/copyright.jsp